Published in final edited form as:
Diabetologia. 2008 December 01; 51(12): 2252–2262. doi:10.1007/s00125-008-1111-z.

Calcium elevations in MIN6 cells evoked by extracellular human islet amyloid polypeptide involve activation of the mechanosensitive ion channel Trpv4

S. Casas[1], **A. Novials**[1], **F. Reimann**[3], **R. Gomis**[1,2], **F.M. Gribble**[3,*]

[1]Endocrinology and Diabetes Unit, Laboratory of Diabetes and Obesity, IDIBAPS-Fundació Clínic, Hospital Clínic, Barcelona, Spain

[2]CIBER de Diabetes y Enfermedades Metabólicas (CIBERDEM), Spain

[3]Cambridge Institute for Medical Research and Department of Clinical Biochemistry, Wellcome Trust/MRC Building, Hills Road, Cambridge, CB2 0XY, UK

Abstract

Aims—To investigate the mechanism by which human islet amyloid polypeptide (hIAPP) fibril formation results in calcium influx across the plasma membrane of pancreatic beta-cells and its association with apoptosis.

Methods—Cytoplasmic calcium concentrations ($[Ca^{2+}]_i$) were monitored for 2 hours as the 340/380 nm fluorescence ratio in fura-2 loaded MIN6-cells. Cell morphology was evaluated by transmission electron microscopy, and viability by FACS analysis.

Results—hIAPP (10 μM) increased $[Ca^{2+}]_i$ in 21% of MIN6 cells in standard buffer, and in 8% of cells in Na^+-free buffer. TRP channel inhibitors (gadolinium, ruthenium red) prevented the Ca^{2+} rise under both conditions, whilst nifedipine was only effective in the presence of Na^+. hIAPP reduced cell viability in both insulinoma and beta cells in primary culture, however, cells were partly rescued by ruthenium red ($p<0.05$),. By RT-PCR, we detected expression of the mechanosensitive TRP channel Trpv4 in MIN6 cells and mouse pancreas. siRNA against Trpv4 prevented hIAPP-induced $[Ca^{2+}]_i$ rises, decreased hIAPP-triggered expression of the ER stress-response, and reduced hIAPP-triggered cell death by 48% ($p<0.05$).

Conclusions—Alterations in $[Ca^{2+}]_i$ play a key role in hIAPP-induced β-cell cytotoxicity. By electron microscopy, we detected extracellular hIAPP aggregates adjacent to irregular invaginated regions of the plasma membrane. We propose that Trpv4 channels may sense physical changes in the plasma membrane induced by hIAPP aggregation, enabling Ca^{2+} entry, membrane depolarization and activation of L-type Ca^{2+} channels. Decreasing the activity of Trpv4 prevented hIAPP-induced $[Ca^{2+}]_i$ changes, reduced hIAPP-triggered ER stress and improved cell viability.

[*]**Corresponding author:** Fiona M. Gribble, Cambridge Institute for Medical Research and Department of Clinical Biochemistry, Wellcome Trust/MRC Building, Hills Road, Cambridge CB2 0XY, UK, Tel: +44 1223 336746, Fax : +44 1223 331206, fmg23@cam.ac.uk.

Duality of Interest
The authors declare that they have not duality of interest to disclose.

Europe PMC Funders Author Manuscripts

Keywords

Amylin; IAPP; amyloid; calcium; plasma membrane; Trpv4; apoptosis

Introduction

Islet amyloid polypeptide (IAPP), also known as amylin, is the main component of islet amyloid (1,2), which is found within the pancreatic islets of Langerhans in subjects with type 2 diabetes mellitus (T2DM) (3,4). Because deposits of islet amyloid colocalize with areas of cell degeneration, the process of amyloidosis has been strongly associated with the progressive loss of pancreatic β-cell mass that is one of the hallmarks of type 2 diabetes (5–8). A target region of human IAPP (hIAPP) between positions 20 and 29 is thought to be responsible for the formation of amyloid fibrils (9). Rodent IAPP (rIAPP), which differs from the human sequence at several residues within this critical region, is not amyloidogenic (9).

The process of ordered aggregation into amyloid fibrils is a common event in many cell-degenerative diseases, including Alzheimer's disease, Pakinson's disease, prion-protein related encephalopathies and several other local and systemic amyloidoses (10). Although the peptides that form amyloid deposits show no apparent primary sequence homology, they all adopt a β-strand secondary structure after conversion to fibrils (11), suggesting that partially folded states serve as the precursors for nucleation (12–14). However, the toxicity of amyloidogenic peptides appears to lie in the oligomeric intermediates rather than the mature fibrils (15,16). Thus, the conversion of a normally soluble protein into amyloid can give rise to a gain in toxic function, providing a common mechanism by which amyloid contributes to disease pathogenesis through cell toxicity and cell death (17).

Amyloid peptides have been reported to induce death cell by apoptosis (6,18–20), which may result from the disruption of calcium homeostasis (21). Indeed, in MIN6 model pancreatic β-cells, we recently showed that hIAPP triggered calcium changes that were associated with the induction of apoptosis via a pathway involving activation of the endoplasmic reticulum (ER) stress response (22). The elevation of intracellular calcium in neurons and astrocytes has been reported to follow the formation and extracellular deposition of several amyloid peptides, including hIAPP (23–27), and a range of potential underlying mechanisms for the increased calcium permeability have been proposed. In cell-free systems such as phospholipid bilayers, hIAPP amyloid has been reported to form cation-permeable channels as a result of its insertion into membranes (28), but also to destabilize the membrane structure in parallel with the measured kinetics of hIAPP fibril growth (29) and to cause a non-specific increase in conductance (16,30–33). In addition, however, activation of cell surface receptors coupled to calcium influx has been reported in a neural cell line exposed to amyloid β peptide aggregation (34). Although diverse, these mechanisms are compatible with the idea that the cytotoxicity of hIAPP is initiated on the cell surface and requires close contact between the aggregation process and the β-cell plasma membrane (6). In regions where this occurs, the plasma membrane of pancreatic β-

Europe PMC Funders Author Manuscripts

cells in amyloidogenic islets *in vivo* is usually characterized by ultrastructural morphological abnormalities (2,35–37).

The aim of the present study was to investigate the mechanism by which hIAPP fibril formation results in calcium influx across the plasma membrane of MIN6 cells and its association with apoptosis.

Methods

Cell culture

The mouse pancreatic β-cell line MIN6 (38) was cultured in Dulbecco's modified Eagle's medium supplemented with 10% fetal bovine serum, 2 mM L-glutamine, 5 μM β-mercaptoethanol, 100 U/ml penicillin and 100 μg/ml streptomycin, at 37°C with 5% CO_2.

Islet isolation and culture

Islets were isolated by collagenase P (Roche Diagnostics, Indianapolis, IN) digestion of the pancreas, and separated from exocrine tissue by Histopaque (Sigma-Aldrich, Steinheim, Germany) density gradient. Islets were transferred to RPMI-1640 medium (Gibco-BRL, Pisley, UK) containing 11.1 mM glucose and supplemented with 10% FBS, 2 mM L-glutamine, 100 U/ml penicillin and 100 μg/ml streptomycin, and cultured at 37°C with 5% CO_2. All procedures were carried out with male mice on pure C57BL/6 background and in accordance with the Institutional Animal Ethics Committee's policies.

Solutions and chemicals

Synthetic human and rat IAPP peptides (Bachem, Bubendorf, Switzerland) were dissolved in sterile water at 500 μM and incubated at room temperature for 10min before use at a final concentration of 10 μM. Drugs and chemicals were purchased from Sigma-Aldrich (Poole, UK) unless otherwise stated, and were added to the bath solutions as indicated. The bath solution for calcium imaging experiments was a Krebs-Ringer bicarbonate solution containing (mM): 149.5 NaCl, 6.5 KCl, 31.2 $NaHCO_3$, 2.7 $MgCl_2$, 4.3 $CaCl_2$, 26 Hepes (pH 7.4), to which 1.3% bovine serum albumin and 1 mM glucose was added. The Na^+ free buffer contained choline+ in place of Na^+.

Transmission electron microscopy

For ultrastructural analysis of insoluble aggregates, a 4 μl sample of the same suspension was applied onto a formvar carbon-coated copper grid for one minute, dried, stained with 2% (w/v) uranyl acetated in water for one minute and air-dried. For cellular ultrastructural analysis, MIN6 cells in culture were fixed in glutaraldehyde 2.5% (w/v) in 0.1 M phosphate buffer (pH 7.4) at 4°C for 1.5 h, rinsed in 0.1 M phosphate buffer and post-fixed in osmium tetroxide 1% (w/v) in the same buffer for 1 h. The samples were dehydrated in an ascending series of acetone concentrations, embedded in Spurr resin and polymerized at 60°C for 48 h. Ultra-thin sections (60-90 nm) were cut using a Reichert-Jung Ultracut E ultramicrotome. They were then placed on 200 mesh copper grids and doubled stained with uranyl acetate (2%) and lead citrate. The grids were examined using a Jeol 1010 transmission electron microscope (Jeol, Tokyo, Japan) operating at an accelerating voltage of 80 kV.

Thioflavin T fluorescence assay

The development of hIAPP fibrils was monitored by Thioflavin T (ThT) fluorescence assay. Each reaction was performed with 5 μM ThT in assay buffer (50 mM Tris, 100 mM KCl, 1 mM EDTA, pH 8.0) containing 10 μM of freshly reconstituted hIAPP or rIAPP peptide. Measurements were recorded at 37°C by using a microplate spectrofluorometer (SpectraMax GeminiXS; Molecular Devices, Sunnyvale, CA). Excitation and emission wavelengths were set at 440 and 482 nm, respectively.

$[Ca^{2+}]_i$ measurements

Cells were plated on glass-bottom dishes (Mattek) 1-3 days prior to use and loaded with fura-2 by incubation in 2 μM of the acetoxymethylester (Molecular Probes, Leiden, Netherlands) for 30 min in bath solution containing 1 mM glucose at room temperature. Measurements were made on an inverted Fluorescence Microscope (Olympus IX71, Southall, UK) with a 40x oil-immersion objective. Excitation at 340 and 380 nm was achieved using a combination of a 75W Xenon arc lamp and a monochromator (Cairn Research, Faversham, UK) controlled by MetaFluor software (Universal Imaging, Cairn) and emission was recorded with a CCD camera (Orca ER, Hammamatsu, Cairn) using a dichroic mirror and a 510 nm long pass filter. Minimal and maximal signals were recorded in the presence of 5 μM ionomycin in 5 mM EGTA/0 mM Ca^{2+} and 5 mM Ca^{2+}, respectively, at the end of the experiment.

RNA interference

Small interference RNA (siRNA) duplexes for mouse transient receptor potential cation channel subfamily V member 4 (Trpv4) and amylase 2 (Amy2) were obtained from Dharmacon (Lafayette, CO). A total of 170 nM of each siRNA duplexes was transfected into MIN6 cells using lipofectamine2000 (Invitrogen, Carlsbad, CA). Cells were processed and analyzed after 48 h of transfection. Cells treated with siAMY2 were used as a negative control. Prior to siRNA experiments, transfection optimization to ensure maximum siRNA uptake was performed with si*GLO*® green fluorescent control reagent (Dharmacon). The efficiency of transfection expressed as the percentage of green fluorescent positive cells was 91.47±6.25% (mean ± SEM from four independent experiments).

RT-PCR

Total RNA was extracted using TRI® reagent (Sigma-Aldrich) following the manufacturer's instructions. Thereafter, cDNA was synthesized from 1 μg of total RNA by using SuperScript™ II RNase H reverse transcriptase (Invitrogen). PCR of 35 amplification cycles was carried out with 50 ng of cDNA and specific oligonucleotide primers using *Taq* DNA polymerase (Promega, Madison, WI). Primers for *Trpv4* were 5'-ATCAACTCGCCCTTCAGAGA-3' and 5'-GGTGTTCTCTCGGGTGTTGT-3', and for β-actin (Actb) were 5'-TGAGAGGGAAATCGTGCGTG-3' and 5'-TGCTTGCTGATCCACATCTGC-3'. PCR products were separated by electrophoresis on a 1.5% agarose gel and visualized by ethidium bromide staining. Primers for analysis of mouse X-box binding factor-1 (*Xbp1*) mRNA splicing were 5'-GAACCAGGAGTTAAGAACACG-3' and 5'-AGGCAACAGTGTCAGAGTCC-3'. PCR

products were separated by electrophoresis on a 2.5% agarose gel and visualized by ethidium bromide staining. Unspliced and spliced *Xbp1* gave products of 205 and 179 bp, respectively. The percentage of *sXbp1* to total *Xbp1* was determined by densitometry using Quantity One software (Bio-Rad Laboratories, Hercules, CA).

Real-time quantitative RT-PCR

Heat shock protein 90kDa beta member 1 (*Hsp90b1*) and *Actb* were amplified using SYBR Green PCR Core Reagents (Applied Biosystems, Warrington, UK) with primers 5'-CACACTAGGTCGTGGAACAACA-3' and 5'-TCTGTCTTGCTACTCCACACGT-3', and 5'-GATCTGGCACCACACCTTCTACA-3' and 5'-CGTCACCGGAGTCCATCACAA-3', respectively. PCR was run with 1 ng cDNA using ABI Prism 7900HT Sequence Detection System (Applied Biosystems) following manufacturer's instructions. A standard curve of each primer set was generated from serial dilutions of cDNA. The PCR products were verified using dissociation curve analysis after run using SDS software (Applied Biosystems). *Actb* values were used to normalize *Hsp90b1* expression.

Apoptosis assay

MIN6 cells were harvested and pooled with their culture medium in order to evaluate also cells that had lost their adherent properties during apoptosis. The protocol for isolation of single islet cells was as published previously (22). Mouse islets were digested in PBS containing 0.125 mg/ml trypsin and 0.05 mg/ml EDTA at 37°C. The cell suspension was cycled for 5 min on ice to allow islets to sediment. The supernatant containing single cells was removed and placed in FBS. To obtain additional single islet cells, the digestion process was repeated three times. Thereafter, cells were stained with annexin V-fluorescein isothiocyanate (FITC) and propidium iodide (PI) using Annexin V-FITC Apoptosis Detection Kit (Becton Dickinson, San Jose, CA) according to the manufacturer's instructions. Samples were analyzed by fluorescence-activated cell sorting (FACS) within one hour on a FACS Calibur with Cell Quest software (Becton Dickinson). FACS gating based on forward and side scatter of 10,000 to 20,000 cells was included for analysis. Annexin V-FITC and PI negative cells were considered as viable, annexin V-FITC positive cells as early apoptotic and those both positive for annexin V-FITC and PI as late apoptotic or dead cells.

Statistical analysis

Data are presented as the mean ± SEM. Comparisons between groups were performed by the *T*-test. Differences in frequencies between groups were assessed by the Chi-square test.

Results

As reported previously, hIAPP was observed to aggregate spontaneously in solution over the course of 2 hours (39). Electron microscopy of freshly prepared solutions containing 10 μM hIAPP showed that prefibrillar hIAPP structures were first observed after 10 min, with maximum formation after 30-45 min (Fig. 1A, left panel). At 2 hours we also detected fibrils of hIAPP (Fig. 1A, right panel). The development of hIAPP fibrils was confirmed by monitoring the fluorescence of ThT at 482 nm, the intensity of which reflects the binding to,

Europe PMC Funders Author Manuscripts

and hence the formation of, amyloid fibrils. In solutions containing 10 μM hIAPP, but not 10 μM rIAPP, ThT fluorescence increased throughout the 2 hour incubations, indicating the progressive formation of fibrils (Fig. 1B).

To investigate whether hIAPP increases cytosolic calcium concentrations in the insulinoma cell line MIN6, we monitored the 340/380 nm fluorescence ratio in cells loaded with the calcium indicator dye, fura-2. When MIN6 cells were incubated in 10 μM hIAPP for 2 hours, we observed a >1.4-fold elevation of the fluorescence ratio in 21.3% of cells (70/328), indicative of a rise in the intracellular calcium concentration (Fig. 2A-C). By contrast, no calcium changes of this magnitude were observed in 128 cells treated with rIAPP or in 87 cells incubated without additions (Fig. 2D,E) (p<0.001 vs hIAPP). In the cells incubated with hIAPP, the latency of the calcium rise had a bimodal distribution, with a first peak occurring at 25-30 min and a second at 75-90 min (Fig. 2B). The timing of the first peak coincides with the first appearance of IAPP deposits by light microscopy. In those cells that exhibited a rise in $[Ca^{2+}]_i$, the 340/380 nm ratio increased progressively until, in many cases, the cell was observed to detach from the glass dish, thereby preventing calibration of the calcium signal in individual responsive cells. The mean peak ratio before detachment in the cells that exhibited a calcium rise was 2.0 ± 0.39 (n=41), similar to the maximum ratio of 1.9 ± 0.54 (n=72) in the remaining cells treated at the end of the experiment with ionomycin and 5 mM Ca^{2+}. This suggests that the calcium concentration in affected cells rose to at least 1 μM.

We next investigated whether the rise in $[Ca^{2+}]_i$ was dependent on calcium entry through voltage gated Ca^{2+} channels. Inclusion of 5 μM nifedipine in the incubation medium significantly abolished the hIAPP-triggered rise in the fura-2 ratio (0/198 cells responded, p<0.001 compared with hIAPP alone) (Fig. 3A), suggesting that L-type Ca^{2+} channels contribute to the calcium rise in MIN6 cells. As L-type Ca^{2+} channels normally only open at a threshold membrane potential of approx -40 mV, the most likely explanation for their recruitment by hIAPP is as a consequence of membrane depolarisation. To investigate the role of Na^+ ions in any initial depolarisation, we repeated the experiments in buffer containing choline$^+$ in place of Na^+. In the absence of hIAPP, the calcium concentration in MIN6 cells was less stable in this Na^+-free buffer, and tended to rise slightly during the 2 hour incubation, with 4/187 cells (2.1%) showing a fluorescence ratio change of >1.4-fold (Fig. 3B). This may be explained by Na^+/Ca^{2+} exchangers operating in reverse when extracellular Na^+ is removed, resulting in persistent Ca^{2+} influx, as described previously in β-cells (40). Removal of extracellular Na^+ did not, however, prevent the larger calcium responses to hIAPP, which were observed in 8.2% of cells (7/85, p<0.01 compared with Na^+-free buffer alone) (Fig. 3C). Interestingly, however, in Na^+-free buffer nifedipine was no longer able to abolish hIAPP-triggered calcium responses, which were still observed in 8.4% of cells (13/154: not significantly different from the response rate with hIAPP in Na^+-free buffer alone) (Fig. 3D). This suggests that under Na^+-free conditions, hIAPP activates a Ca^{2+} influx pathway distinct from the opening of L-type Ca^{2+} channels.

The results raised the possibility that a non voltage-dependent Ca^{2+} channel, such as a TRP channel, might be implicated in responses to hIAPP, and we speculated that a mechanosensitive member of the TRP channel family might play a role. To test this

hypothesis, we first investigated the effect of the relatively non-specific TRP channel inhibitor, gadolinium (Gd^{3+}, 100 μM). In support of our hypothesis, addition of Gd^{3+}, in the presence of Na^+ free buffer and nifedipine, abolished the calcium responses to hIAPP (0.3% responders, 1/311 cells, $p<0.001$ compared with hIAPP in Na^+ free buffer without Gd^{3+}) (Fig. 3E).

We next examined our microarray database (41) for mechanosensitive TRP channels expressed in MIN6 cells, and the search identified the Ca^{2+}-permeable channel Trpv4 as a possible candidate. To investigate the potential role of Trpv4, we tested the effect of Ruthenium Red (RR), a general inhibitor of TRPV channels. Both in standard buffer and Na^+ free buffer, RR (10 μM) abolished the effect of hIAPP on $[Ca^{2+}]_i$ (only 0.6% of cells responded in standard bath and 1% responded in Na^+ free buffer, $p<0.001$ compared with hIAPP in standard or Na^+-free buffer without RR, respectively) (Fig. 3F,G).

By electron microscopy, we observed that hIAPP aggregates interacted with the cell membrane of MIN6 cells early after treatment (Fig. 4A). In these regions, the plasma membrane became irregular and exhibited membrane protrusions, which were clearly evident after 2 hours. hIAPP-induced membrane changes were also observed in the presence of RR, indicating that the effect of RR was not to prevent membrane changes or fibril formation (Fig. 4A).

To study the downstream effect of hIAPP cytotoxicity, we measured apoptosis by FACS analysis. Cells incubated for 24 hours in the presence of hIAPP exhibited only 68% viability compared with control cells (cf 93% viability using rIAPP) (Fig. 4B). Addition of RR in the presence of hIAPP improved cell viability to 79% ($p=0.006$), representing a 45% reduction in hIAPP-induced cell death (Fig. 4B). We next investigated whether we could confirm the key observed effects of RR on hIAPP cytotoxicity in primary cultures of mouse pancreatic islets (Fig.4C). After 72 hours treatment with 10 μM hIAPP, viability of mouse islet cells decreased significantly to 22% compared to 73% in the control ($p<0.001$) (Fig. 4D). Treatment with RR in the presence of hIAPP improved islet cell viability to 45% ($p<0.05$), representing a 52% reduction in hIAPP-induced apoptosis (Fig. 4D).

We further evaluated the potential involvement of Trpv4 in hIAPP- triggered calcium changes and apoptosis using siRNA technology. By RT-PCR, we detected *Trpv4* expression in MIN6 cells, as well as liver, testis and pancreas (Fig. 5A). Transient transfection of MIN6 cells with siRNA against Trpv4 (siTrpv4) decreased expression of *Trpv4*, as assessed by RT-PCR, whereas the control siRNA against amylase (siAmy2) had no effect on *Trpv4* expression (Fig. 5B). When fura-2-loaded, siAmy2-treated MIN6 cells were incubated in hIAPP for 2 hours, elevation of the 340/380 nm fluorescence ratio was detected in 10% of cells (14/156), whereas siTrpv4-treated cells showed a significant protection against hIAPP induced $[Ca^{2+}]_i$ elevation (0.87% responders, **x/y** cells,: $p<0.001$ compared with siAmy2) (Fig. 5C).

We also investigated whether silencing the Trpv4 gene had a protective effect on hIAPP-induced apoptosis, by measuring cell viability after 24 hours of hIAPP treatment. In the apoptosis assay using FACS, cell viability was ~78% in control cells transfected with either

siAmy2 or siTrpv4. Whilst hIAPP reduced viability in the control siAmy2 cells to 26%, it only decreased viability to 52% in the siTrpv4 cells (p=0.002 for comparison between siAmy2 and siTrpv4 cells each treated with hIAPP). This represents a 50% reduction in hIAPP-triggered cell death by apoptosis in the cells with reduced expression of Trpv4 (Fig. 5D).

Recent findings revealed that the hIAPP-triggered calcium elevation and apoptosis in MIN6 cells were associated with activation of the ER stress response (22). To attempt to distinguish between the possibilities that hIAPP-induced ER stress might be either a trigger of, or a consequence of, the observed cytoplasmic [Ca^{2+}] changes, we assessed the degree of ER stress in siTrpv4-treated cells, as these exhibited significantly reduced hIAPP-triggered [Ca^{2+}] changes. ER stress was quantified by measuring the activation of Xbp1. The spliced active form of *Xbp1* is a key transcription factor for upregulation of ER chaperones during ER stress responses (42), and has been shown to be important for maintenance of pancreatic β-cell ER function (43). Splicing of *Xbp1* mRNA in MIN6 cells under control conditions was 23.24±1.9% of the total *Xbp1* (Fig. 5E). Exposure of siAmy2-treated cells to 10 μM hIAPP for 2 hour significantly increased the levels of *sXbp1* to 41.26±3.23% (p<0.05 *vs* basal condition), however, no increment was observed in cultures treated with siTrpv4 (21.35±2.14% of total *Xbp1*) (Fig. 5E). Twenty-four hours after treatment, the increase of *sXbp1* product had returned near to basal levels in siAmy2 and remained normal in siTrpv4-treated cells (30.25±4.4% and 20.64±0.42%, respectively) (Fig. 5E). Moreover, we studied the expression level of *Hsp90b1*, which encodes a resident ER luminal molecular chaperone, known to be elevated by the upstream activity of *sXbp1* as a consequence of ER stress (42). siAmy2-treated cells incubated in the presence of hIAPP showed significantly increased expression of *Hsp90b1* after both 2 and 24 hours (p=0.02 and p=0.01 at 2 and 24 hours, compared with untreated siAmy2 cells). In cells treated with siTrpv4 and incubated with hIAPP, expression of *Hsp90b1* was normal at 2 and 24 hours (Fig. 5F). These data represent a significant reduction in hIAPP-triggered ER stress in the cells with reduced expression of Trpv4 (Fig. 5E-F), which is in agreement with the observed protection against hIAPP-triggered cell death (Fig. 5D).

Discussion

Our results show that hIAPP triggers calcium changes in a model of the pancreatic β-cell, the MIN6 cell line. Calcium elevation was progressive and severe, and frequently resulted in cell detachment. The calcium changes corresponded in time with the appearance of hIAPP aggregates in the solution, alterations in the surface membrane morphology, and a reduction in cell viability. Pharmacological and siRNA experiments suggested that activation of both Trpv4 and L-type calcium channels contributed to the hIAPP-triggered calcium rise.

The synthetic IAPP peptide concentration used in the present study is within the range of concentrations used in the literature to spontaneously form IAPP oligomers and fibrils in culture (6,9,16,22). In T2DM, IAPP fibrils are often found accumulated between β-cells and islet capillaries (2,35–37), indicating that there may be insufficient clearance of secreted IAPP, making it difficult to estimate the IAPP concentrations that accumulate locally throughout the years of disease progression. Nevertheless, we showed here that the

ultrastructural morphology of MIN6 cells in the amyloidogenic conditions was characterized by plasma membrane alterations compared with the control cells. These alterations included cell membrane irregularities and invaginations filled with fibrils, similar to those described in human T2DM islets *in vivo* (2,35–37).

Amyloid oligomers (including hIAPP) have been reported to increase [Ca^{2+}] in neurons and astrocytes (23–27), although the effect of hIAPP on pancreatic β-cells is not well documented. We showed recently that increases in intracellular [Ca^{2+}] could be detected in hIAPP-treated MIN6 cells, with associated activation of the ER stress response and induction of apoptosis (22). An earlier study, by contrast, suggested that hIAPP does not trigger changes in [Ca^{2+}] in insulinoma cells (44), but the conclusions were derived from measurements of [Ca^{2+}] in cell populations which might have excluded any non-attached cells. Our finding that individual MIN6 cells detached soon after experiencing a hIAPP-triggered Ca^{2+} rise might explain the previous failure to detect Ca^{2+} changes in insulinoma cells.

The mechanisms previously implicated in calcium responses to amyloid oligomers in other cell types and cell-free systems include direct formation of Ca^{2+}-permeable pores by the amyloid oligomers themselves and the activation of voltage gated calcium channels (28,34). Amyloid-pores are unlikely to underlie our findings in MIN6 cells, as the Ca^{2+} changes were inhibited by nifedipine, Gd^{3+} and ruthenium red, none of which has been found to block amyloid channels. The inhibition of hIAPP-triggered Ca^{2+} responses by nifedipine in MIN6 cells indicated, however, that L-type Ca^{2+} channels were activated by hIAPP, either as a result of changes in the properties of the L-type Ca^{2+} channels themselves, or as a secondary consequence of membrane depolarisation. The latter idea is supported by the findings in Na^{+}-free buffer, as an additional nifedipine-insensitive Ca^{2+}-elevating pathway was identified under these conditions. This was found to be blocked by Gd^{3+} or ruthenium red, indicating the likely involvement of specific members of the TRP channel family. siRNA mediated knock down of the mechanosensitive TRP channel, Trpv4, protected against the toxic effects of hIAPP on [Ca^{2+}] as well as on induction of ER stress and apoptosis. Our subsequent Trpv4 knock down experiments, using loss of cell viability as a marker of hIAPP-induced apoptosis, supported the notion that activation of this channel may be an early response to hIAPP.

Trpv4 is a mechano- and osmo-sensitive channel located on the cell surface, with a Ca^{2+}/Na^{+} permeability ratio of ~6 (45), which is inhibited by Gd^{3+} and ruthenium red, and is not blocked by 2-APB. The observed morphological deformations in the plasma membrane following hIAPP treatment suggest that the deposition of hIAPP insoluble aggregates, which can reach high molecular weights (46), might weaken the mechanical strength of the plasma membrane making it susceptible to Trpv4 activation. We propose that it may provide a link between hIAPP-induced mechanical perturbations of the β-cell plasma membrane by hIAPP and the depolarising Ca^{2+} influx. The finding that siTrpv4 protected against both hIAPP-induced ER stress and [Ca^{2+}] changes suggests that this channel is involved at a step that precedes the ER stress response, perhaps at the level of cytoplasmic [Ca^{2+}] modulation. However, as RR did not protect completely against amyloid cytotoxicity, our data cannot exclude the involvement of other early mechanisms in the induction of islet amyloid

cytotoxicity. Nevertheless, activation of Trpv4 may play a more widespread role in mediating some of the effects of amyloid on intracellular [Ca^{2+}] that have been previously described in the literature. Amyloid-induced Ca^{2+} entry has, for example, been attributed to activation of channels with a relatively high selectivity for Ca^{2+} over Na^{+} (47), which are insensitive to L-type Ca^{2+} channel blockers (48). The potential involvement of Trpv4 and alternative mechanosensitive channels in mediating amyloid-induced Ca^{2+} changes, ER stress and apoptosis in other cell types will require further evaluation.

Acknowledgements

Study sponsored by Sardà Farriol Research Program, and supported by FIS (PI05/1215), REDIMET (RD06/0015) and CIBER de Diabetes y Enfermedades Metabólicas (CIBERDEM) initiatives of ISCIII from *Ministerio de Sanidad y Consumo*, and by SGR2005/00019 grant from *Generalitat de Catalunya* in Spain. S.C. is recipient of a *Juan de la Cierva* contract from *Ministerio de Educación y Ciencia* in Spain and thanks the award of an Albert Renold Fellowship from the European Foundation for the Study of Diabetes. F.M.G. is supported by the Wellcome Trust, and F.R. by St John's College, Cambridge.

Abbreviations

Actb	β-Actin
Amy2	Amylase 2
$[Ca^{2+}]_i$	Intracellular calcium concentration
ER	Endoplasmic Reticulum
hIAPP	human Islet Amyloid Polypeptide
Hsp90b1	Heat shock protein 90kDa beta member 1
PI	Propidium Iodide
rIAPP	rodent Islet Amyloid Polypeptide
RR	Ruthenium Red
siRNA	small interference RNA
T2DM	Type 2 diabetes mellitus
ThT	Thioflavin T
TRP	Transient receptor potential
Trpv4	TRP cation channel subfamily V member 4

References

1. Westermark P, Wernstedt C, Wilander E, Hyden DW, O'Brien TD, Johnson KH. Amyloid fibrils in human insulinoma and islets of Langerhans of the diabetic cat are derived from a neuropeptide-like protein also present in normal islet cells. Proc Natl Acad Sci USA. 1987; 84:3881–3885. [PubMed: 3035556]

2. Clark A, Cooper GJ, Lewis CE, Morris JF, Willis AC, Reid KB, Turner RC. Islet amyloid formed from diabetes-associated peptide may be pathogenic in type-2 diabetes. Lancet. 1987; 2:231–234. [PubMed: 2441214]
3. Westermark P, Grimelius L. The pancreatic islet cells in insular amyloidosis in human diabetic and non-diabetic adults. Acta Pathol Microbiol Scand A. 1973; 81:291–300. [PubMed: 4129056]
4. Howard CF Jr. Longitudinal studies on the development of diabetes in individual Macaca nigra. Diabetologia. 1986; 29:301–306. [PubMed: 3522329]
5. Hull RL, Westermark GT, Westermark P, Kahn SE. Islet amyloid: a critical entity in the pathogenesis of type 2 diabetes. J Clin Endocrinol Metab. 2004; 89:3629–3643. [PubMed: 15292279]
6. Lorenzo A, Razzaboni B, Weir GC, Yankner BA. Pancreatic islet cell toxicity of amylin associated with type-2 diabetes mellitus. Nature. 1994; 368:756–760. [PubMed: 8152488]
7. Janson J, Soeller WC, Roche PC, Nelson RT, Torchia AJ, Kreutter DK, Butler PC. Spontaneous diabetes mellitus in transgenic mice expressing islet amyloid polypeptide. Proc Natl Acad Sci USA. 1996; 93:7283–7288. [PubMed: 8692984]
8. Butler AE, Jang J, Gurlo T, Carty MD, Soeller WC, Butler PC. Diabetes due to a progressive defect in β-cell mass in rats transgenic for human islet amyloid polypeptide (HIP rat). A new model for type 2 diabetes. Diabetes. 2004; 53:1509–1516. [PubMed: 15161755]
9. Westermark P, Engström U, Johnson KH, Westermark GT, Betsholtz C. Islet amyloid polypeptide: Pinpointing amino acid residues linked to amyloid fibril formation. Proc Natl Acad Sci USA. 1990; 87:5036–5040. [PubMed: 2195544]
10. Westermark P, Benson MD, Buxbaum JN, Cohen AS, Frangione B, Ikeda S, Masters CL, Merlini G, Saraiva MJ, Sipe JD. Nomenclature Committee of the International Society of Amyloidosis. Amyloid toward terminology clarification. Report from the Nomenclature Committee of the International Society of Amyloidosis. Amyloid. 2005; 12:1–4. [PubMed: 16076605]
11. Cohen AS, Calkins E. Electron microscopic observations on a fibrous component in amyloid of diverse origins. Nature. 1959; 183:1202–1203. [PubMed: 13657054]
12. Conway KA, Harper JD, Lansbury PT. Accelerated in vitro fibril formation by a mutant alpha-synuclein linked to early-onset Parkinson disease. Nat Med. 1998; 4:1318–1320. [PubMed: 9809558]
13. Walsh DM, Hartley DM, Kusumoto Y, Fezoui Y, Condron MM, Lomakin A, Benedek GB, Selkoe DJ, Teplow DB. Amyloid beta-protein fibrillogenesis. Structure and biological activity of protofibrillar intermediates. J Biol Chem. 1999; 274:25945–25952. [PubMed: 10464339]
14. Kayed R, Bernhagen J, Greenfield N, Sweimeh K, Brunner H, Voelter W, Kapurniotu A. Conformational transitions of islet amyloid polypeptide (IAPP) in amyloid formation in vitro. J Mol Biol. 1999; 287:781–796. [PubMed: 10191146]
15. Lambert MP, Barlow AK, Chromy BA, Edwards C, Freed R, Liosatos M, Morgan TE, Rozovsky I, Trommer B, Viola KL, Wals P, et al. Diffusible, nonfibrillar ligands derived from Abeta1-42 are potent central nervous system neurotoxins. Proc Natl Acad Sci USA. 1998; 95:6448–6453. [PubMed: 9600986]
16. Janson J, Ashley RH, Harrison D, McIntyre S, Butler PC. The mechanism of islet amyloid polypeptide toxicity is membrane disruption by intermediate-sized toxic amyloid particles. Diabetes. 1999; 48:491–498. [PubMed: 10078548]
17. Kayed R, Head E, Thompson JL, McIntire TM, Milton SC, Cotman CW, Glabe CG. Common structure of soluble amyloid oligomers implies common mechanism of pathogenesis. Science. 2003; 300:486–489. [PubMed: 12702875]
18. Yankner BA, Duffy LK, Kirschner DA. Neurotrophic and neurotoxic effects of amyloid beta protein: reversal by tachykinin neuropeptides. Science. 1990; 250:279–282. [PubMed: 2218531]
19. Forloni G, Angeretti N, Chiesa R, Monzani E, Salmona M, Bugiani O, Tagliavini F. Neurotoxicity of a prion protein fragment. Nature. 1993; 362:543–546. [PubMed: 8464494]
20. Tanaka Y, Engelender S, Igarashi S, Rao RK, Wanner T, Tanzi RE, Sawa A, Dawson V, Dawson TM, Ross CA. Inducible expression of mutant alpha-synuclein decreases proteasome activity and increases sensitivity to mitochondria-dependent apoptosis. Hum Mol Genet. 2001; 10:919–926. [PubMed: 11309365]

21. Mattson MP, Chan SL. Calcium orchestrates apoptosis. Nat Cell Biol. 2003; 5:1041–1043. [PubMed: 14647298]
22. Casas S, Gomis R, Gribble FM, Altirriba J, Knuutila S, Novials A. Impairment of the ubiquitin-proteasome pathway is a downstream endoplasmic reticulum stress response induced by extracellular human islet amyloid polypeptide and contributes to pancreatic beta-cell apoptosis. Diabetes. 2007; 56:2284–2294. [PubMed: 17563070]
23. Mattson MP, Cheng B, Davis D, Bryant K, Lieberburg I, Rydel RE. beta-Amyloid peptides destabilize calcium homeostasis and render human cortical neurons vulnerable to excitotoxicity. J Neurosci. 1992; 12:376–389. [PubMed: 1346802]
24. Mattson MP, Goodman Y. Different amyloidogenic peptides share a similar mechanism of neurotoxicity involving reactive reactive oxygen species and calcium. Brain Res. 1995; 676:219–224. [PubMed: 7796173]
25. Kawahara M, Kuroda Y, Arispe N, Rojas E. Alzheimer's beta-amyloid, human islet amylin, and prion protein fragment evoke intracellular free calcium elevations by a common mechanism in a hypothalamic GnRH neuronal cell line. J Biol Chem. 2000; 275:14077–14083. [PubMed: 10799482]
26. Abramov AY, Canevari L, Duchen MR. Changes in intracellular calcium and glutathione in astrocytes as the primary mechanism of amyloid neurotoxicity. J Neurosci. 2003; 23:5088–5095. [PubMed: 12832532]
27. Demuro A, Mina E, Kayed R, Milton SC, Parker I, Glabe CG. Calcium dysrerugulation and membrane disruption as a ubiquitous neurotoxic mechanism of soluble amyloid oligomers. J Biol Chem. 2005; 280:1794–17300.
28. Mirzabekov TA, Lin MC, Kagan BL. Pore formation by the cytotoxic islet amyloid peptide amylin. J Biol Chem. 1996; 271:1988–1992. [PubMed: 8567648]
29. Engel MF, Khemtémourian L, Kleijer CC, Meeldijk HJ, Jacobs J, Verkleij AJ, de Kruijff B, Killian JA, Höppener JW. Membrane damage by human islet amyloid polypeptide through fibril growth at the membrane. Proc Natl Acad Sci USA. 2008; 105:6033–6038. [PubMed: 18408164]
30. Kayed R, Sokolov Y, Edmonds B, McIntire TM, Milton SC, Hall JE, Glabe CG. Permeabilization of lipid bilayers is a common conformation-dependent activity of soluble amyloid oligomers in protein misfolding diseases. J Biol Chem. 2004; 279:46363–46366. [PubMed: 15385542]
31. Knight JD, Miranker AD. Phospholipid catalysis of diabetic amyloid assembly. J Biol Chem. 2004; 341:1175–1187.
32. Green JD, Kreplak L, Goldsbury C, Li Blatter X, Stolz M, Cooper GS, Seelig A, Kistler J, Aebi U. Atomic force microscopy reveals defects within mica supported lipid bilayers induced by the amyloidogenic human amylin peptide. J Biol Chem. 2004; 342:877–887.
33. Sparr E, Engel MFM, Sakharov DV, Sprong M, Jacobs J, Kruijff B, Hoppener JWM, Killian JA. Islet amyloid polypeptide-induced membrane leakage involves uptake of lipids by forming amyloid fibers. FEBS Letters. 2004; 577:117–120. [PubMed: 15527771]
34. Blanchard BJ, Chen A, Rozeboom LM, Stafford KA, Weigele P, Ingram VM. Efficient reversal of Alzheimer's disease fibril formation and elimination of neurotoxicity by a small molecule. Proc Natl Acad Sci USA. 2004; 101:14326–14332. [PubMed: 15388848]
35. Westermark P. Fine structure of islets of Langerhans in insular amyloidosis. Virchows Arch A Pathol Pathol Anat. 1973; 359:1–18. [PubMed: 4632997]
36. Westermark P, Engström U, Westermark GT, Johnson KH, Permerth J, Betsholtz C. Islet amyloid polypeptide (IAPP) and pro-IAPP immunoreactivity in human islets of Langerhans. Diabetes Res Clin Pract. 1989; 7:219–226. [PubMed: 2691219]
37. Sempoux C, Guiot Y, Dubois D, Moulin P, Rahier J. Human type 2 diabetes: morphological evidence for abnormal beta-cell function. Diabetes. 2001; 50(Suppl. 1):S172–S177. [PubMed: 11272184]
38. Ishihara H, Asano T, Tsukuda, Katagiri H, Inukai K, Anai M, Kikuchi M, Yazaki Y, Miyazaki JI, Oka Y. Pancreatic β-cell line MIN6 exhibits characteristics of glucose metabolism and glucose-stimulated insulin secretion similar to those of normal islets. Diabetologia. 1993; 36:1139–1145. [PubMed: 8270128]

39. Kayed R, Bernhagen J, Greenfield N, Sweimeh K, Brunner H, Voelter W, Kapurniotu A. Conformational transitions of islet amyloid polypeptide (IAPP) in amyloid formation in vitro. J Mol Biol. 1999; 287:781–796. [PubMed: 10191146]
40. Van Eylen F, Bollen A, Herchuelz A. NCX1 Na/Ca exchanger splice variants in pancreatic islet cells. J Endocrinol. 2001; 168:517–526. [PubMed: 11241183]
41. [Accessed 12 April 2005] NCBIs Gene Expression Omnibus series accession number GSE2253. Available from http://www.ncbi.nlm.nih.gov/geo/
42. Eizirik DL, Cardozo AK, Cnop M. The role for endoplasmic reticulum stress in diabetes mellitus. Endocr Rev. 2008; 29:42–61. [PubMed: 18048764]
43. Nozaki J, Kubota H, Yoshida H, Naitoh M, Goji J, Yoshinaga T, Mori K, Koizumi A, Nagata K. The endoplasmic reticulum stress response is stimulated through the continious activation of transcription factors ATF6 and XBP1 in Ins2+/Akita pancreatic β-cells. Genes Cells. 2004; 9:261–270. [PubMed: 15005713]
44. Bai JZ, Saafi EL, Zhang S, Cooper GJS. Role of Ca^{2+} in apoptosis evoked by human amylin in pancreatic islet β-cells. Biochem J. 1999; 343:53–61. [PubMed: 10493911]
45. Strotmann R, Harteneck C, Nunnenmacher K, Schultz G, Plant TD. OTRPC4, a nonselective cation channel that confers sensitivity to extracellular osmolarity. Nat Cell Biol. 2000; 2:695–702. [PubMed: 11025659]
46. Goldsbury C, Goldie K, Pellaud J, Seelig J, Frey P, Müller SA, Kistler J, Cooper GJ, Aebi U. Amyloid fibril formation from full-length and fragments of amylin. J Struct Biol. 2000; 130:352–362. [PubMed: 10940238]
47. Abramov AY, Canevari L, Duchen MR. Calcium signals induced by amyloid beta peptide and their consequences in neurons and astrocytes in culture. Biochim Biophys Acta. 2004; 1742:81–87. [PubMed: 15590058]
48. Abramov AY, Canevari L, Duchen MR. Changes in intracellular calcium and glutathione in astrocytes as the primary mechanism of amyloid neurotoxicity. J Neurosci. 2003; 23:5088–5095. [PubMed: 12832532]

Europe PMC Funders Author Manuscripts

Europe PMC Funders Author Manuscripts

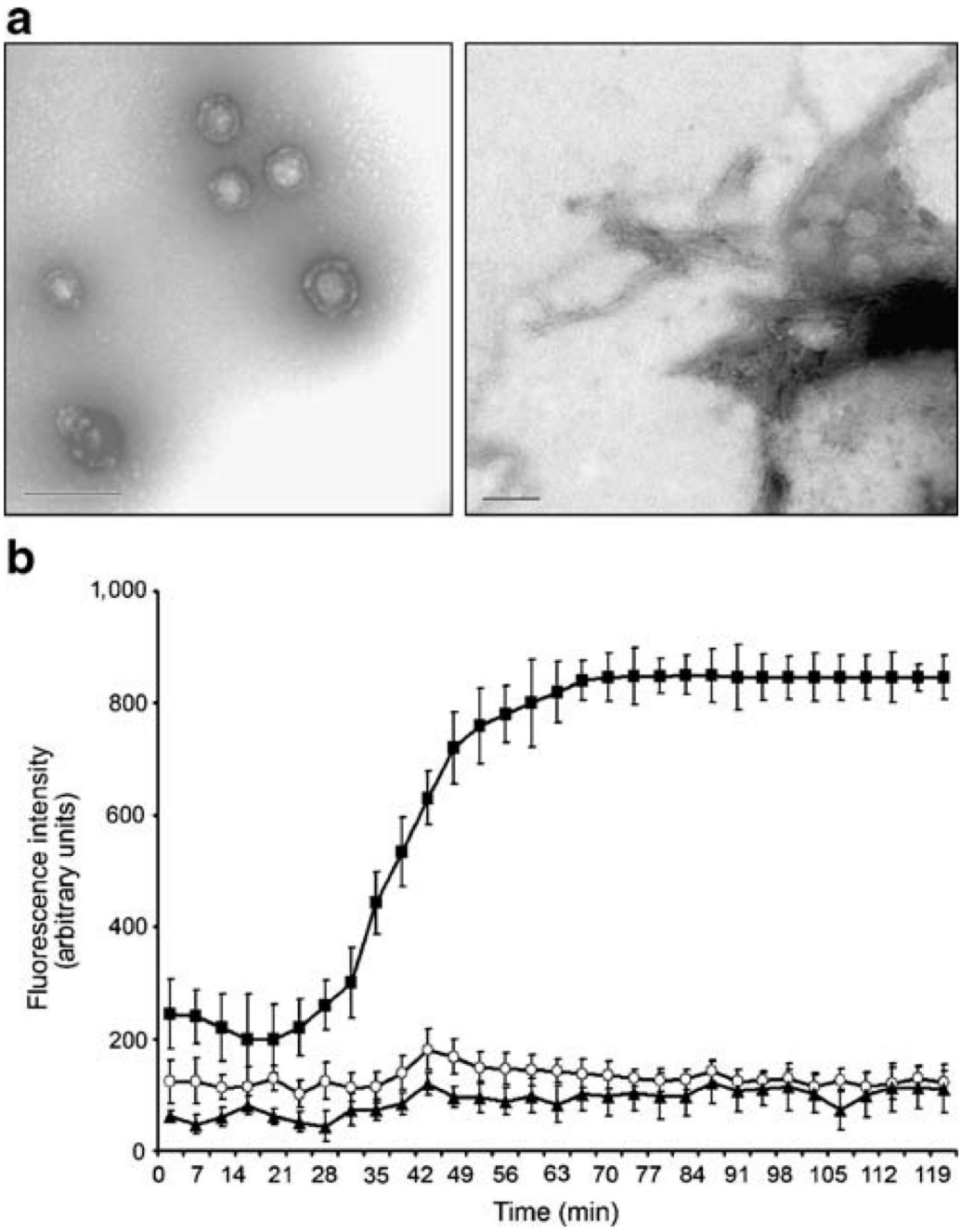

Figure 1. Human IAPP aggregation process

(**A**) Electron microscopy images showing spontaneous aggregation of 10 μM hIAPP. Prefibrillar hIAPP structures were first observed after 10 min, and maximum formation was achieved after 30-45 min (left panel). hIAPP fibrils were detected at 2 h (right panel). Magnifications are indicated. (**B**) ThT binding assay. Formation of hIAPP fibrils was monitored over time by the fluorescence intensity of ThT. Experiments were performed with either 10 μM hIAPP or rIAPP (n=8).

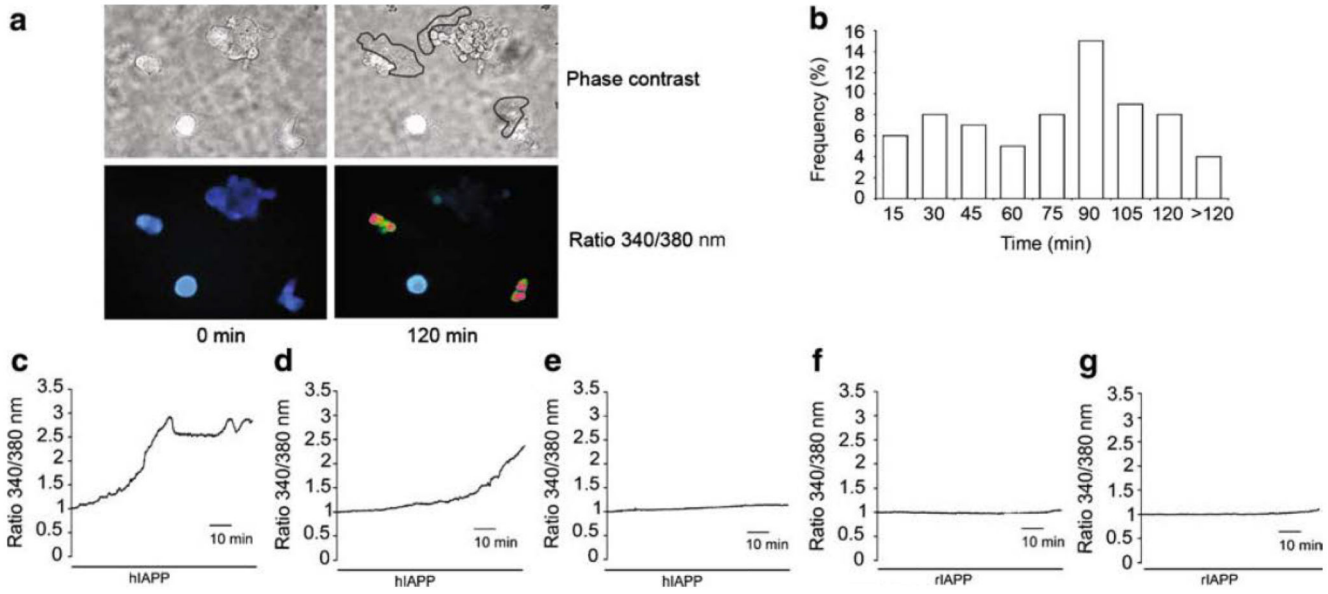

Figure 2. Effect of human and rat IAPP on $[Ca^{2+}]_i$ in MIN6 cells

(**A**) $[Ca^{2+}]_i$ was monitored for 2 h as the 340/380 nm fluorescence ratio in fura-2 loaded MIN6 cells. Treatment with 10 μM hIAPP led to the formation of insoluble aggregates (outlined) after 30-45 min and was associated with an increase in 340/380 nm fluorescence ratio. Image representative of 12 independent experiments from different cell preparations. (**B**) Frequency histogram of the latencies of Ca^{2+} responses in the 21.34% of hIAPP-treated MIN6 cells that exhibited a rise in the 340/380 nm fluorescence ratio (n=328 cells, 12 independent experiments). Latency was measured as the time to achieve a 1.4 fold increase in fluorescence ratio. Latencies were binned into 15 min intervals, and are labeled with the time at the end of the respective 15 min period.

(**C**) Representative traces of early responsive (<60 min) (left plot), late responsive (>60 min) (central plot) and unresponsive (right plot) MIN6 cells treated with 10 μM hIAPP. Traces are representative of 12 independent experiments from different cell preparations (n=328).

(**D**) No appreciable increase in 340/380 nm fluorescence ratio was observed in MIN6 cells treated with 10 μM rIAPP. Trace is representative of 2 independent experiments from different cell preparations (n=128).

(**E**) $[Ca^{2+}]_i$ monitored in MIN6 cells in buffer without IAPP. Trace is representative of 4 independent experiments from different cell preparations (n=87).

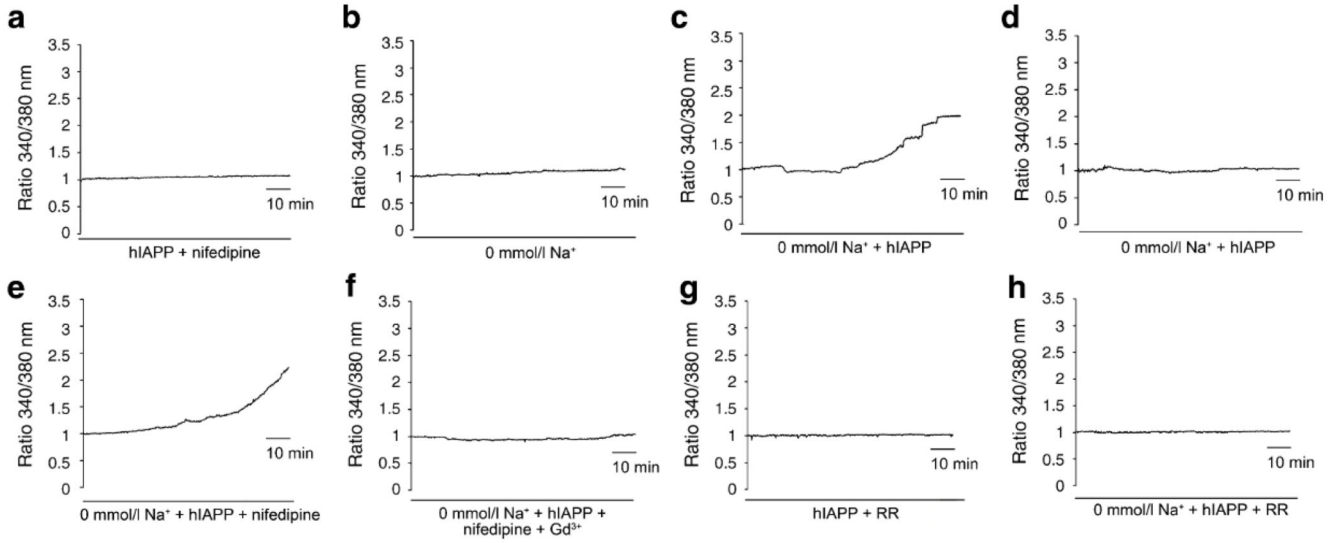

Figure 3. Effect of Na^+, nifedipine, gadolinium and ruthenium red on $[Ca^{2+}]_i$ changes induced by 10 μM hIAPP in MIN6 cells

(**A**) No appreciable increase in $[Ca^{2+}]_i$ was observed in MIN6 cells treated with 10 μM hIAPP and 5 μM nifedipine for 2 hours. Trace is representative of 4 independent experiments from different cell preparations (n=198).

(**B**) In Na^+-free buffer, $[Ca^{2+}]_i$ was stable for 2 hours in 97.9% (183/187) of MIN6 cells in the absence of hIAPP. Trace is representative of 4 independent experiments from different cell preparations (n=187).

(**C**) In Na^+-free buffer, 10 μM hIAPP treatment increased $[Ca^{2+}]_i$ in 8.2% of MIN6 cells (7/85). Representative traces of a responsive and a non-responsive cell are shown, taken from 2 independent experiments on different cell preparations (n=85).

(**D**) In Na^+-free buffer, administration of 5 μM nifedipine could not prevent the increases in $[Ca^{2+}]_i$ triggered by 10 μM hIAPP, which were still observed in 8.4% of MIN6 cells (13/154). Trace is representative of a responsive cell taken from 2 independent experiments on different cell preparations (n=154).

(**E**) In Na^+-free buffer, $[Ca^{2+}]_i$ was stable in 99.7% of cells (310/311) when 100 μM Gd^{3+} was added in the presence of 10 μM hIAPP and 5 μM nifedipine. Trace is representative of 3 independent experiments from different cell preparations (n=311).

(**F,G**) In the presence of 10 μM ruthenium red (RR) and 10 μM hIAPP, $[Ca^{2+}]_i$ remained stable in 99.4% of MIN6 cells (340/342) in standard bath solution (**F**), and in 98.8% of cells (169/171) in Na^+-free buffer (**G**). Traces are representative of 4 independent experiments from different cell preparations in each buffer.

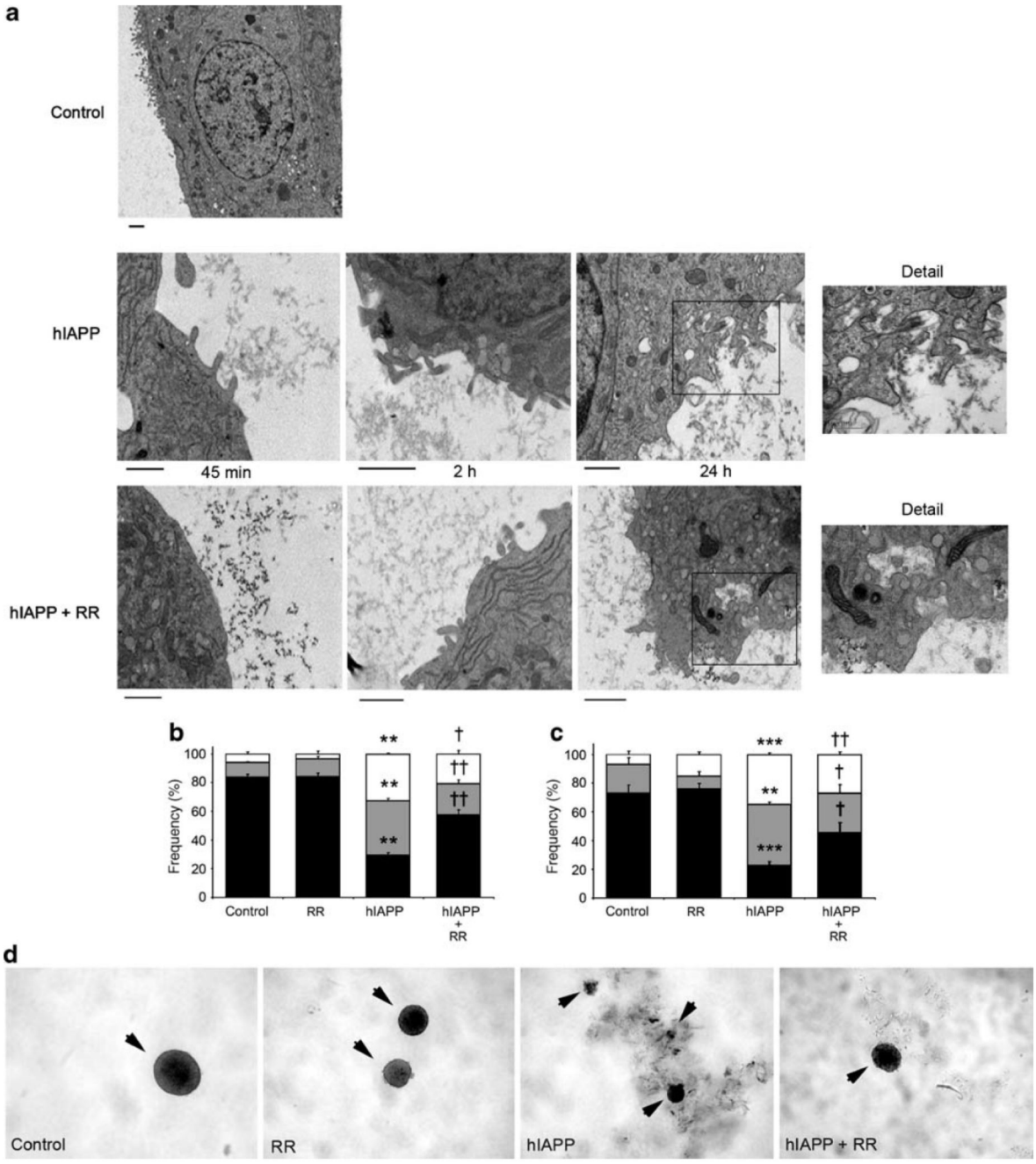

Figure 4. Effect of 10 μM ruthenium red on cell morphology and viability induced by 10 μM hIAPP in MIN6 cells

(**A**) MIN6 cells treated with 10 μM hIAPP were studied over time by electron microscopy. Images revealed that extracellular hIAPP insoluble forms were in close contact with the plasma membrane of MIN6 cells. In these regions, the plasma membrane became irregular, and at 24 hours deep invaginations were observed both in the absence and presence of 10 μM (RR). The scale bar represents 1 μm in each image.

(**B**) Apoptosis assay of MIN6 cells treated for 24 hours with 10 μM hIAPP and/or 10 μM RR compared with control, measured by annexin V-FITC plus PI staining and FACS analysis. Results are mean ± SEM (n=6). *, $p<0.001$ compared with control; †, $p<0.01$ and ††, $p<0.001$ compared with 10 μM hIAPP.

(**C**) Mouse pancreatic islets (arrowheads) were cultured for 72 hours with 10 μM hIAPP and/or 10 μM RR compared with control. Treatment with 10 μM hIAPP led to the formation of insoluble aggregates that were in contact with islet borders. Note the disintegration of the islet shape in islets incubated with hIAPP versus control. Representative images (10x magnification). (**D**) Apoptosis assays were performed on dispersed islet cells following treatments as above, by staining with annexin V-FITC plus PI and FACS analysis. Results are mean ± SEM (n=6). *, $p<0.01$ and **, $p<0.001$ compared with control; †, $p<0.05$ and ††, $p<0.01$ compared with 10 μM hIAPP.

Europe PMC Funders Author Manuscripts

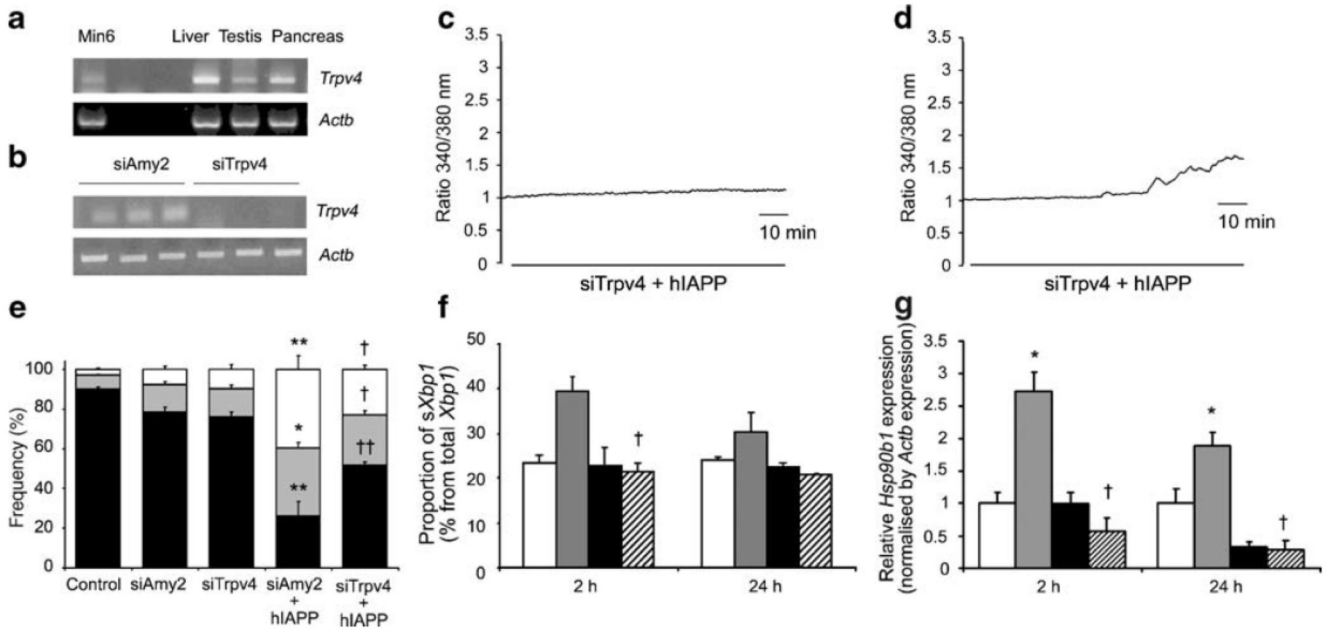

Figure 5. Expression of *Trpv4* and protective effects of siTrpv4 in the presence of 10 μM hIAPP

(**A**) Representative electrophoresis gel images showing PCR amplification products corresponding to *Trpv4* and *Actb* expression in MIN6 cells and mouse liver, testis and pancreas.

(**B**) siRNA duplexes for mouse *Trpv4* were transfected into MIN6 cells at 170 nM. After 48 hours, cells were treated with or without 10 μM hIAPP for a further 24 hours. Cells treated with siAmy2 were used as a negative control. Representative electrophoresis gel images showing PCR amplification products corresponding to *Trpv4* and *Actb* expression in MIN6 cells following siRNA treatments.

(**C**) In the presence of 10 μM hIAPP for 2 hours, $[Ca^{2+}]_i$ remained stable in 99% (229/231) of siTrpv4-transfected MIN6 cells (upper plot), but increased in 10% (14/156) of siAmy2-transfected MIN6 cells (lower plot). Traces are representative of 5 independent experiments from different cell preparations in each condition.

(**D**) Apoptosis assay performed on MIN6 cells transfected with siAmy2 or siTrpv4, and treated for 24 hours with or without 10 μM hIAPP compared with control (non-transfected, untreated cells). Cells were stained with annexin V-FITC plus PI and analyzed by FACS. Results are mean ± SEM (n=6). *, $p<0.01$ and **, $p<0.001$ compared to siAmy2; †, $p<0.05$ and ††, $p<0.01$ compared to siAmy2 with 10 μM hIAPP.

(**E**) RT-PCR analysis of *Xbp1* splicing was performed on MIN6 cells transfected with siAmy2 or siTrpv4, and treated with or without 10 μM hIAPP for 2 and 24 hours using primers flanking the intron excised from mouse *Xbp1* mRNA. The percentage of *sXbp1* to total *Xbp1* determined by densitometry is illustrated. Data are mean ± SEM (n=6) *; $p<0.05$ compared to siAmy2; †, $p<0.05$ compared to siAmy2 with 10 μM hIAPP.

(**F**) Induction of *Hsp90b1* expression, a marker of ER stress, measured by real-time quantitative RT-PCR on MIN6 cells transfected with siAmy2 or siTrpv4, and treated with or

Europe PMC Funders Author Manuscripts

without 10 μM hIAPP for 2 and 24 hours. Results are mean ± SEM (n=6). *, $p<0.05$ compared to siAmy2; †, $p<0.01$ compared to siAmy2 with 10 μM hIAPP.

Europe PMC Funders Author Manuscripts